The Astrophysical Journal, 876:85 (13pp), 2019 May 1 https://doi.org/10.3847/1538-4357/ab1422

Large Magellanic Cloud Cepheid Standards Provide a 1% Foundation for the Determination of the Hubble Constant and Stronger Evidence for Physics beyond ΛCDM

Adam G. Riess[1,2], Stefano Casertano[1,2], Wenlong Yuan[2], Lucas M. Macri[3], and Dan Scolnic[4]
[1] Space Telescope Science Institute, 3700 San Martin Drive, Baltimore, MD 21218, USA
[2] Department of Physics and Astronomy, Johns Hopkins University, Baltimore, MD 21218, USA
[3] Texas A&M University, Department of Physics and Astronomy, College Station, TX 77845, USA
[4] Duke University, Department of Physics, Raleigh, NC 27708, USA
Received 2019 March 18; revised 2019 March 25; accepted 2019 March 26; published 2019 May 7

Abstract

We present an improved determination of the Hubble constant from *Hubble Space Telescope (HST)* observations of 70 long-period Cepheids in the Large Magellanic Cloud (LMC). These were obtained with the same WFC3 photometric system used to measure extragalactic Cepheids in the hosts of SNe Ia. Gyroscopic control of *HST* was employed to reduce overheads while collecting a large sample of widely separated Cepheids. The Cepheid period–luminosity relation provides a zero-point-independent link with 0.4% precision between the new 1.2% geometric distance to the LMC from detached eclipsing binaries (DEBs) measured by Pietrzyński et al. and the luminosity of SNe Ia. Measurements and analysis of the LMC Cepheids were completed prior to knowledge of the new DEB LMC distance. Combined with a refined calibration of the count-rate linearity of WFC3-IR with 0.1% precision, these three improved elements together reduce the overall uncertainty in the geometric calibration of the Cepheid distance ladder based on the LMC from 2.5% to 1.3%. Using only the LMC DEBs to calibrate the ladder, we find $H_0 = 74.22 \pm 1.82\,\mathrm{km\,s^{-1}\,Mpc^{-1}}$ including systematic uncertainties, 3% higher than before for this particular anchor. Combining the LMC DEBs, masers in NGC 4258, and Milky Way parallaxes yields our best estimate: $H_0 = 74.03 \pm 1.42\,\mathrm{km\,s^{-1}\,Mpc^{-1}}$, including systematics, an uncertainty of 1.91%–15% lower than our best previous result. Removing any one of these anchors changes H_0 by less than 0.7%. The difference between H_0 measured locally and the value inferred from Planck CMB and ΛCDM is $6.6 \pm 1.5\,\mathrm{km\,s^{-1}\,Mpc^{-1}}$ or 4.4σ ($P = 99.999\%$ for Gaussian errors) in significance, raising the discrepancy beyond a plausible level of chance. We summarize independent tests showing that this discrepancy is not attributable to an error in any one source or measurement, increasing the odds that it results from a cosmological feature beyond ΛCDM.

Key words: cosmological parameters – distance scale – stars: variables: Cepheids – supernovae: general

Supporting material: machine-readable tables

1. Introduction

Cepheid variables in the Magellanic Clouds (Leavitt & Pickering 1912; Hertzsprung 1913) have long played a starring role in the distance scale and the determination of the present value of the expansion rate of the universe, the Hubble constant (H_0). With knowledge of the distance to the Large Magellanic Cloud (LMC), our nearest Cepheid-rich neighbor, we can directly determine the absolute magnitudes of these pulsating stars. Cepheids have been observed with the *Hubble Space Telescope (HST)* in the hosts of SNe Ia at distances of up to ~20 Mpc with WFPC2 (Freedman et al. 2001; Sandage et al. 2006) and up to ~40 Mpc with ACS and WFC3 (Riess et al. 2016) to measure the far greater luminosities of these exploding stars. The resulting ability to determine distances to SNe Ia deep into the Hubble–Lemaître flow completes a distance ladder that provides the most precise, model-independent, and direct means for determining H_0. Knowledge of this cosmological parameter remains central to describing the present state of our universe and setting expectations for its fate.

In addition to characterizing the state of our universe, refined measurements of H_0 may also be pointing toward a new wrinkle in the cosmological model. Measurements of the distance ladder with improved precision and control of systematics from the SH0ES Team (Riess et al. 2016, hereafter R16) demonstrate that the universe is expanding at present about 9% faster than inferred from the ΛCDM model calibrated by Planck CMB data (Planck Collaboration et al. 2018) from the early universe, with a significance of 3.6σ (Riess et al. 2018a, hereafter R18a). The higher local value results from the use of any one of five independently determined, geometric distance estimators used to determine the luminosity of Cepheids, including masers in NGC 4258 (Humphreys et al. 2013; Riess et al. 2016), eight detached eclipsing binaries (DEBs) in the LMC (Pietrzyński et al. 2013), and three distinct approaches to measuring Milky Way (MW) parallaxes (Benedict et al. 2007), with the most recent from *HST* spatial scanning (Riess et al. 2018b, hereafter R18b) and *Gaia* DR2 (R18a). Further out, the distance ratios to SN Ia hosts provided by Cepheids have been confirmed to a precision of 2%–3% by a dozen measured with the Tip of the Red Giant Branch (Jang & Lee 2017; Jang et al. 2018; Hatt et al. 2018a, 2018b) and Miras (Huang et al. 2018; Yuan et al. 2017; C. Huang et al. 2019, in preparation). Strong-lensing results from the H0LiCOW team (Birrer et al. 2018) are fully independent of all rungs of the distance ladder yet find a similar value of H_0 from the late universe, one that is 2.3σ ($P = 98\%$) higher than the Planck-calibrated value. At the other end of time, the low value of H_0 predicted from the early

universe is corroborated by independent measurements of the CMB or Ω_B with baryon acoustic oscillation (BAO) data (Addison et al. 2018) and from "inverse distance ladders," such as the one built by the Dark Energy Survey that is calibrated from the sound horizon at $z \sim 1000$ (Macaulay et al. 2019, see Discussion for further consideration of these results). With multiple, independent checks now established at both ends of cosmic history, this "H_0 Tension" between the early and late universe, as it is widely known, may be interpreted as evidence for a new cosmological feature such as exotic dark energy, a new relativistic particle, dark matter-radiation or neutrino-neutrino interactions, dark matter decay, or a small curvature, each producing a different-sized shift (Khosravi et al. 2017; Renk et al. 2017; Aylor et al. 2018; D'Eramo et al. 2018; Di Valentino et al. 2018; Mörtsell & Dhawan 2018; Barenboim et al. 2019; Kreisch et al. 2019; Pandey et al. 2019; Vattis et al. 2019) with some proposals spanning the full discrepancy while improving the agreement between the model and CMB data (Poulin et al. 2018). Pinpointing the cause of the tension requires further improvement in the local measurements, with continued focus on precision, accuracy, and experimental design to control systematics.

New measurements of 20 late-type DEBs in the LMC from Pietrzyński et al. (2019) offer the most precise foundation to date to geometrically calibrate this distance ladder. The current approach to measuring these geometric distances uses long-baseline near-infrared (NIR) interferometry of individual late-type giants to measure their angular sizes and derives a purely empirical relation between their surface brightness and color relation, with a scatter of only 0.018 mag. That such a relation exists is a direct consequence of the Planck Law. Applying this relation to a late-type giant in a DEB system yields the geometrically calibrated angular diameter of the star from its color and brightness. Combining the physical radius derived from radial velocities and eclipsing light curves yields a purely geometric distance with a typical precision of ∼2% per system. These DEB measurements appear quite robust, as the variance of the sample is fully characterized by the method and there is no dependence on astrophysical models; the details can be found in Pietrzyński et al. (2013, 2019). The most recent result uses an improved surface brightness and color, whose calibration otherwise systematically limits the measurement, and an expanded sample of 20 DEBs to measure the distance to the center of the LMC to 1.2% (0.0263 mag) precision.

To fully exploit the improved precision of the LMC distance, we need greater control of systematic errors than past measurements. Simply comparing the brightnesses of Cepheids in the LMC to those in SN Ia hosts measured from two different telescopes would incur a net systematic 2%–3% error, just from the use of different photometric systems with their individual zero-point uncertainties. Measurements of Cepheids in the NIR are especially important in order to mitigate systematic errors from extinction and metallicity variations. Yet photometric errors are larger in the NIR, as ground-based bandpasses are unstable and are redefined nightly by the atmosphere. Even for the best calibrated ground-based system in the NIR, 2MASS, the *systematic* uncertainty in the transformation to the best-match WFC3 *F160W* band (after accounting for bandpass differences) is found empirically to be $\sigma \approx 0.03$–0.04 mag (Riess 2011). This is not surprising, as the *absolute* zero-points of each are (claimed to be) known to only 0.02–0.03 mag (Skrutskie et al. 2006; Kalirai et al. 2009). Thus, mixing ground-based photometry from Cepheids in the NIR from (Macri et al. 2015, hereafter M15) or Persson et al. (2004) with those from *HST* in SN Ia hosts incurs a ∼1.4%–1.8% systematic error in distance measurements, swamping the improved LMC distance precision unless a single, stable system is used to measure both sets of Cepheids and nullify zero-point errors. Even using a single photometric system, it is necessary to calibrate its ability to measure relative fluxes across the 10 mag range between Cepheids in the LMC and SN Ia hosts. Fortunately, concurrent work has now calibrated the linearity of the WFC3-IR detector to a precision of 2.4 mmag across this range, making the higher precision sought feasible (Calamida et al. 2018; Narayan et al. 2019; Bohlin & Deustua 2019; Riess et al. 2019).

In the past, the prospect of observing many Cepheids in the LMC directly with *HST* was hampered by the high cost of observatory overheads. Because the LMC is nearby, its Cepheids are far apart in angle, and thus observing each with *HST* required a dedicated pointing (with attendant guide star acquisition overhead). However, using a newly available commanding and control sequence under purely gyroscopic control called "DASH" (Drift And SHift; Momcheva et al. 2017), we observed up to a dozen LMC Cepheids in three filters in a single orbit, obtaining *HST* photometry for 70 widely separated LMC Cepheids with WFC3 in three filters. This photometry establishes a new, zero-point-independent link between LMC Cepheids and those in the hosts of SNe Ia.

In Section 2 we present the observations and measurements of these LMC Cepheid standards, their *P*–*L* relations in Section 3, and the impact on the Hubble constant in Section 4. We consider systematics related to the determination of H_0 in Section 5. We point out that all the photometric measurements of the LMC Cepheids presented here were completed and this manuscript was finalized in advance of the availability of the new LMC distance, its uncertainty, and the revised geometry of the LMC based on the new DEBs measurements in Pietrzyński et al. (2019). After this became available, only the final determination of H_0 was completed.

2. LMC Cepheid Standards

2.1. DASHing through the LMC

The 70 LMC Cepheids presented here were imaged in three bands, two in the optical with WFC3-UVIS (*F555W* and *F814W*) and one in the NIR with WFC3-IR (*F160W*), in two *HST* programs: GO-14648 and GO-15146 (PI: Riess). All data frames are available in MAST.[5] The observations were taken between 2017 January 9 and 2018 December 16 and are identified and described in Table 1.

Measuring the mean magnitudes of a large number of Cepheids in the LMC with the narrow-angle instruments on *HST* poses unique challenges. The mean separation of $P > 6$ day LMC Cepheids is $\sim 10'$ ($\sim 15'$ for $P > 10$ day Cepheids), well in excess of the full $2'$ WFC3 field of view, so in almost all cases only a single Cepheid can be observed per image. Although the necessary exposures times are only a few seconds, with normal observing procedures, each Cepheid observation requires a new fine guidance sensor guide star acquisition with an overhead of 6 minutes, by far the longest interval in the observation. In addition, WFC3 can hold only

[5] MAST is the archive site for STScI and *HST* at /https://mast.stsci.edu.

Table 1
Observations of LMC Cepheids

Cepheid	Frame	Filter	MJD[a]	Exptime (s)	Array	*X*	*Y*
OGL0434	idi532e4q	*F555W*	1357.849	2.00	UVIS	608	515
OGL0434	idi532e5q	*F814W*	1357.850	2.00	UVIS	613	509
OGL0434	idi518iaq	*F160W*	1176.417	2.22	IRSUB256	138	136
OGL0434	idi532dqq	*F160W*	1357.776	2.22	IRSUB256	138	139

Note.
[a] MJD-57,000.0.

(This table is available in its entirety in machine-readable form.)

one full UVIS frame in memory before requiring a memory buffer dump, which requires 350 s. Thus, full-frame imaging of LMC Cepheids with short exposures is extremely inefficient and time consuming; given the demand for the use of *HST*, such observations are unlikely to be undertaken.

However, we can observe these Cepheids far more efficiently by using the new DASH mode of observing, available since Cycle 24 (2016), which uses the *HST* gyroscopes for both slewing and guiding. This mode is highly efficient for our short integrations of 2–2.5 s; during this time, the smearing of the point-spread function (PSF) from the expected gyro drift of 1–2 mas s^{-1} is $\sim 0\farcs003$, which is negligible compared to the $0\farcs04$ size of pixels in WFC3-UVIS or the $0\farcs128$ pixels for WFC3-IR, thereby saving the overhead of repeated guide star acquisitions. By selecting groupings of Cepheids, typically within less than a degree, it is possible to slew *HST* 5′–10′ between successive Cepheids with an overhead of 2 minutes per slew, observe each on a subarray in the NIR, flip the channel select mechanism no more than once per orbit (an observatory requirement), reverse the path, and observe each target again in two optical filters (also in subarray mode), collecting up to 12 Cepheids in three filters in one orbit–and without exceeding the memory buffer. This strategy requires that the accumulated pointing error during the orbit remain smaller than half the subarray size ($\sim 10''$), which is consistent with the aforementioned *expected* gyro drift under normal conditions. Ground-based light curves can be used to adjust each single-epoch magnitude to the epoch of mean intensity as done in R18a and R18b. By definition, these phase corrections are zero-point-independent because they are calculated relative to the average magnitudes of each Cepheid (R18).

Our first attempt at implementing this observing sequence, visit 8 of GO-14648, succeeded as planned on 2017 January 1, collecting the images of 12 LMC Cepheids spread over 0.5 degrees in three bands, 36 exposures in all, obtained within a single *HST* orbit (just over 1 hour of elapsed time). The accumulated drift from the commanded position did not exceed $6''$, and we observed a mean drift of 1.2 mas s^{-1} (see Figure 1); thus, all Cepheids landed well inside their chosen apertures. We selected a sample of 100 LMC Cepheids from the sample of M15, assigning greater priority to Cepheids with longer periods (better analogs of those in SN Ia hosts) and those requiring shorter slews.

Unfortunately, the start of this program and its follow-on, GO-15146, coincided with a period of *severe* degradation in the performance of *HST* Gyro 2, which caused its typical drift rate to exceed its nominal value by more than an order of magnitude. The specific size and direction of the gyro drift at any point in time was found to be highly unpredictable. To

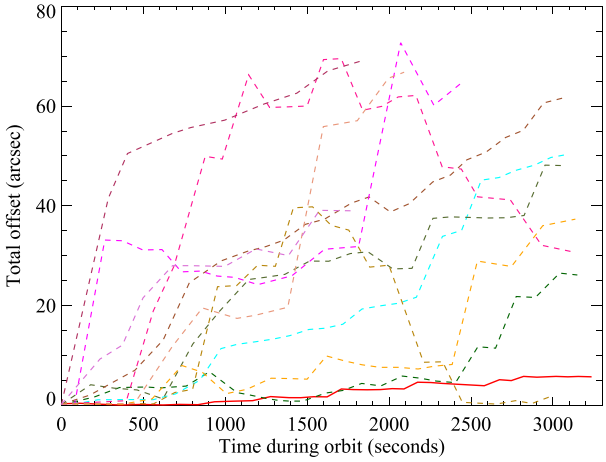

Figure 1. Gyro drift. Each line shows the drift between the commanded position and the encountered in a single orbit under the "DASH" protocol of gyroscopic control. The filled line shows the first result, near the expectation, and before the onset of degradation of gyro 2. The others occurred during the usage of the degraded gyro 2.

overcome increasing gyro drift rates with time, we redesigned our subsequent observations to use larger subarrays and thus provide greater margin for erratic gyro slewing. The larger frames required more onboard memory for storage, and in this state we could observe ∼6–10 Cepheids before filling the memory. By mid-2018, Gyro 2 drifts increased so that the accumulated pointing errors under gyro control reached $20''$–$70''$ after 2000 s (see Figure 1), in some cases exceeding the radius of the full WFC3 frame and thus ensuring that the target would miss the field regardless of the array size used. A few targets were subsequently observed under fine guidance sensor control to complete the intended three bands of imaging. We concluded the observing program with 70 completed targets each with three colors, somewhat less than the 100 targets expected with nominal gyro performance, but representing only a net 17% loss in the statistical power of the sample. Gyro 2 stopped operating at the end of this program and was replaced in the operational chain by Gyro 3, which may have elevated noise; it is unclear how this mode will perform in the new gyro configuration. Should *HST* drop to fewer than three gyro controls, the feasibility of DASH-mode observations is unlikely.

The erratic gyro slewing also made it challenging to determine exactly where *HST* was pointed in each subarray and, thus, where the target star was located (under gyro control, *HST* cannot use the astrometry of a known guide star to establish the pointing coordinates). We developed and

employed an algorithm for matching the apparent positions of stars to a catalog of the LMC to identify the location of each target. The X and Y pixel positions of each Cepheid in the observation as they actually occurred are given in Table 1.

2.2. Photometry

We measured the photometry of the Cepheids using small apertures with radii of 3 pixels for WFC3-UVIS and WFC3-IR to reduce source contamination (from cosmic rays or nearby stars) and to minimize sky noise. Aperture photometry has other advantages over PSF fitting for this application, including lower systematics if the inner PSF varies (which could potentially result from gyro drifts) and less variation from PSF undersampling in single frames. In practice, we did not find any measurable variation in the size or shape of the PSF due to gyro drifts. During the period of degraded Gyro 2 performance, the measured mean drift rate for targets landing in the arrays was 5 mas s^{-1} (with a peak of 13 mas s^{-1}). The corresponding mean drift over the 2.5 s exposure was 0.3 pixels for WFC3-UVIS and 0.1 pixels for WFC3-IR, well within the aperture and compensated by the use of an aperture correction between $r = 3$ and $r = 10$ pixels derived from the mean of all Cepheid PSFs.

Measurements were made on the fully calibrated frames from the MAST archive, using the charge transfer efficiency (CTE)-corrected frames for WFC3-UVIS images. Each calibrated image was multiplied by the pixel area map, a necessary step to obtain correct point-source photometry for an image flat-fielded to constant flux per unit area. For WFC3-UVIS data, we derived and applied an aperture correction from 3 to 10 pixel radius (0.″12–0.″4) in order to utilize the 10 pixel zero-point provided by STScI for each UVIS CCD. Our subarrays all used CCD2, for which the adopted zero-points (magnitude of a star which produces 1 e^{-} s^{-1}) are 25.727 mag for $F555W$ and 24.581 mag for $F814W$ (Vega system). This procedure matches the calibration used for optical Cepheid photometry in R16 and Hoffmann et al. (2016), and the application to the distance scale remains independent of the accuracy of these zero-points as long as the same consistent value is used to measure all Cepheids along the distance ladder.

For WFC3-IR $F160W$, we used aperture corrections of 0.063 mag from a radius of 10 pixels to infinity (provided by STScI) or equivalently 0.200 mag from a 3 pixel radius aperture (measured by us). We adopted a zero-point of 24.71 mag at infinite radius (Vega system), derived to yield the same mean photometry whether measured from these apertures on the original frames or from PSF fitting on resampled images, which is the methodology employed by R16 and Riess et al. (2011, hereafter R11) for SN Ia host images using a scale of 0.″08 $pixel^{-1}$ and a flux drop fraction of 0.6. R16 and R11 used images of the CALSPEC reference star P330 as the reference for the shape and scale of the PSF; this is also one of the stars used to set the zero-point by STScI and has a color similar to that of Cepheids. As a result, the zero-point we derived to ensure uniformity of Cepheid photometry matches the official STScI result to 0.01 mag. By comparing photometry measured with apertures on the original pixel scale and PSF fitting on the resampled images used by R16, we estimate a systematic uncertainty between measurement techniques of 3 mmag.

We also found a small systematic difference in the WFC3-UVIS photometry of Shutter A versus Shutter B images for these very short exposures. Sahu et al. (2014) established that Shutter B causes extra instrument vibrations and can affect the PSF and move some flux outside the aperture for very short exposure times. We determined and corrected for a difference of ±6 mmag in $F555W$ and ±3.5 mmag in $F814W$ depending on which shutter was used.

Next, we applied a correction for the expected difference between the magnitude of each Cepheid at the observed phase and the magnitude at the epoch of mean intensity of its light curve. These phase corrections are derived from ground-based light curves of each Cepheid in filters with wavelengths best corresponding to the WFC3 filters. Because the phase corrections are relative quantities, they do not change the zero-point of the light curves, which remain on the *HST* WFC3 natural system.[6] We derived and applied these phase corrections following the same methodology described in R18b. The periods and phases for $F555W$ and $F814W$ were determined using the V- and I-band light curves from OGLE surveys (Szymanski 2005; Udalski et al. 2008, 2015). For some Cepheids (OGL0434, OGL0501, OGL0510, OGL0512, OGL0528, OGL0545, OGL0590, OGL0712, OGL0757, OGL0966, and OGL0992), we also included V-band light curves from the ASAS survey (Pojmanski 1997) and/or ASAS-SN survey (Shappee et al. 2014; Kochanek et al. 2017) to increase the baseline coverage. We made use of the J- and H-band light curves from M15 and Persson et al. (2004) to correct the $F160W$ random phased measurements to mean intensity. The standard deviations of these corrections are 0.29, 0.17, and 0.11 mag in $F555W$, $F814W$, and $F160W$, respectively, decreasing with the smaller light-curve amplitudes at redder wavelengths. Phase corrections also account for the difference between the Cepheid light-curve magnitude mean (the average of many measured magnitudes) and the magnitude at the epoch of mean intensity (the standard convention for distance measurements). This expected difference is consistent with our sample average correction of −0.048, −0.013, and −0.001 mag, in $F555W$, $F814W$, and $F160W$, respectively. The uncertainties in these phase corrections depend on the quality of the ground-based light curves; the average uncertainty is 0.013, 0.008, and 0.029 mag per epoch in $F555W$, $F814W$, and $F160W$, respectively, which dominates over the statistical photometry errors (i.e., photon statistics) in a single epoch. The differences between repeat measurements for the same target, available for a subset of 19 epochs and filters, is consistent with these uncertainties. The final mean individual uncertainty for these 70 Cepheids is 0.016, 0.012, and 0.029 mag in $F555W$, $F814W$, and $F160W$, respectively. The final mean photometry for each Cepheid in three colors is given in Table 2.

For distance measurements and for the determination of H_0, it is useful to combine these three bands into the same single, reddening-free Wesenheit index (Madore 1982) used by R16 for measuring extragalactic Cepheids in SN Ia hosts:

$$m_H^W = m_{F160W} - 0.386(m_{F555W} - m_{F814W}). \quad (1)$$

where the value of 0.386 is derived from the reddening law of Fitzpatrick (1999) with $R_V = 3.3$. R16 and Follin & Knox (2018) considered a broader range of reddening laws.

[6] In practice, the ground-based light curves are transformed to the *HST* system using color terms. While an uncertainty in color term could produce systematic errors, these are negligible. We determined empirically that a 10% error in the color terms changes the mean phase correction by $\leqslant$0.1 mmag.

Table 2
Photometric Results LMC Cepheids

Cepheid	R.A.	Decl.	Geo	log Period	$F555W$	σ	$F814W$	σ	$F160W$[a]	σ	$m_H^{W,b}$	σ
OGL0434	74.114583	−69.379611	0.028	1.482	13.131	0.028	12.208	0.011	11.321	0.018	10.966	0.021
OGL0501	74.462625	−69.958250	0.034	1.367	13.623	0.022	12.693	0.012	11.770	0.021	11.406	0.023
OGL0510	74.523208	−69.454333	0.027	1.566	13.457	0.037	12.299	0.021	11.232	0.042	10.787	0.045
OGL0512	74.545000	−69.949694	0.033	1.595	13.134	0.025	12.005	0.017	11.038	0.017	10.598	0.020
OGL0528	74.636583	−70.346028	0.038	1.553	13.175	0.052	12.156	0.021	11.226	0.020	10.824	0.029
OGL0545	74.696292	−70.061583	0.034	1.199	14.414	0.045	13.349	0.010	12.311	0.018	11.895	0.025
OGL0590	74.921417	−69.456111	0.025	1.502	13.470	0.025	12.382	0.014	11.311	0.038	10.895	0.039

Notes.
[a] Does not include addition of 0.0300 ± 0.0024 mag to correct CRNL 4 dex between MW and extragalactic Cepheids.
[b] Includes subtraction of geometric correction to LMC line of nodes and addition of 0.0300 ± 0.0024 mag to correct CRNL 4 dex between MW and extragalactic Cepheids.

(This table is available in its entirety in machine-readable form.)

Using the Wesenheit magnitude thus defined has the additional benefit of tightening the resultant *P–L* relation, because across the instability strip, intrinsically redder Cepheids are fainter. For a *P–L* that is well-sampled across the intrinsic color range, the difference in the color ratio for dust and intrinsic color has no impact on relative distance measurements, because the intrinsic component cancels out when comparing the *P–L* relations of different hosts. The m_H^W values for our 70 targets have an individual mean uncertainty of 0.030 mag, including photometric measurement errors, phase corrections, and error propagation to the Wesenheit magnitude.

We can also compare the *P–L* relations we obtain from *HST* photometry with ground-based results, by transforming the ground (*V*, *I*, and *H*) magnitudes from M15 to the *HST* natural system ($F555W$, $F814W$, and $F160W$) via the equations given in R16. We emphasize that this transformation is primarily for comparison purposes and is not required in the calibration of the Cepheid *P–L* in the *HST* photometric system. The results are shown in Figure 2, where we excluded three Cepheids, OGLE0712, OGLE1539, and OGLE1677, whose *HST* images reveal a relatively bright and nearby star ($\Delta\mathrm{mag} < 3$, $\Delta r < 1''$) that would significantly contaminate ground-based photometry of the Cepheid for typical ground-based image quality. We find mean differences (in the direction Ground—*HST*) and sample dispersions (SDs) of 0.036 and 0.030 mag in $F555W$, 0.018 and 0.036 mag in $F814W$, −0.032 and 0.039 mag in $F160W$, and −0.040 and 0.040 mag in m_H^W. There are a couple of outliers in the comparison between space and the ground (two of 67 in each filter); these are marked in Figure 2. These mean differences in zero-points are similar to those found when comparing ground and *HST* magnitudes of MW Cepheids in Riess et al. (2018a): 0.024 mag for $F555W$, 0.038 mag for $F814W$, −0.056 mag for $F160W$, and −0.051 mag for m_H^W. While the dispersion between these ground and *HST* zero-points for this LMC sample is 0.04 mag, the dispersion between these differences for the LMC and MW is <0.02 mag, suggesting these *HST*-to-ground zero-point differences are primarily systematic. The presence of systematic errors in zero-points from either space or ground facilities reinforces the value of maintaining a single, stable photometric system to nullify these errors along the distance ladder.

A comparison of NIR photometry of Cepheids along the distance ladder, even within the same photometric system, must also account for another systematic difference that appears when measuring bright and faint sources with HgCdTe detectors. This effect, called Count-Rate Nonlinearity (CRNL) or reciprocity failure, is different from the more commonly considered nonlinearity of *total* measured counts (often approaching saturation), which is already corrected in the MAST pipeline through calibrations determined from varying the length of integrations. In contrast, CRNL causes photons at low count rates to be detected or collected less efficiently than photons at high count rate, regardless of the length of the exposure.

Recently, Riess et al. (2019) derived a more precise characterization of the CRNL of WFC3 through a combination of comparisons of cluster star photometry between WFC3-IR and WFC3-UVIS at overlapping wavelengths and by comparing observed and synthetic magnitudes of white dwarfs (Calamida et al. 2018; Narayan et al. 2019) and by further extending the results to brighter count rates. Combining these results with previous measurements and those from the WFC3 grism (Bohlin & Deustua 2019) provides a consistent and improved characterization of the CRNL of WFC3-IR, of 0.75 ± 0.06% per dex, with no apparent wavelength dependence, now measured across 16 astronomical magnitudes. This improves by a factor of 4 on the previous measurement of 1.00 ± 0.25% per dex (Riess 2010).

The correction for CRNL is more properly (i.e., physically) considered as accounting for dimming of fainter sources (e.g., Cepheids in SN Ia hosts) relative to brighter sources (such as *HST* reference stars) as a result of charge trapping. However, because calculations involving the distance ladder are only sensitive to the difference in measured flux and because the photometry of the faint Cepheids in SN Ia hosts in R16 did not (by convention) include a correction for CRNL, we account for the net difference here. We have therefore added to the m_H^W photometry in Table 2 the 0.0300 ± 0.0024 mag mean correction to the the bright LMC Cepheids to account for the 4.0 dex flux ratio in $F160W$ between these LMC Cepheids and the sky-dominated Cepheids observed in SN Ia hosts and NGC 4258. This is the same convention used for the MW Cepheids measured with *HST* and presented in R18.

Finally, because of the inclination of the LMC, we expect some Cepheids to be closer or farther than average by a few hundreths of a magnitude in distance modulus, depending on their projected distance from the LMC line of nodes. Pietrzyński et al. (2019) used the DEBs to constrain a tilted

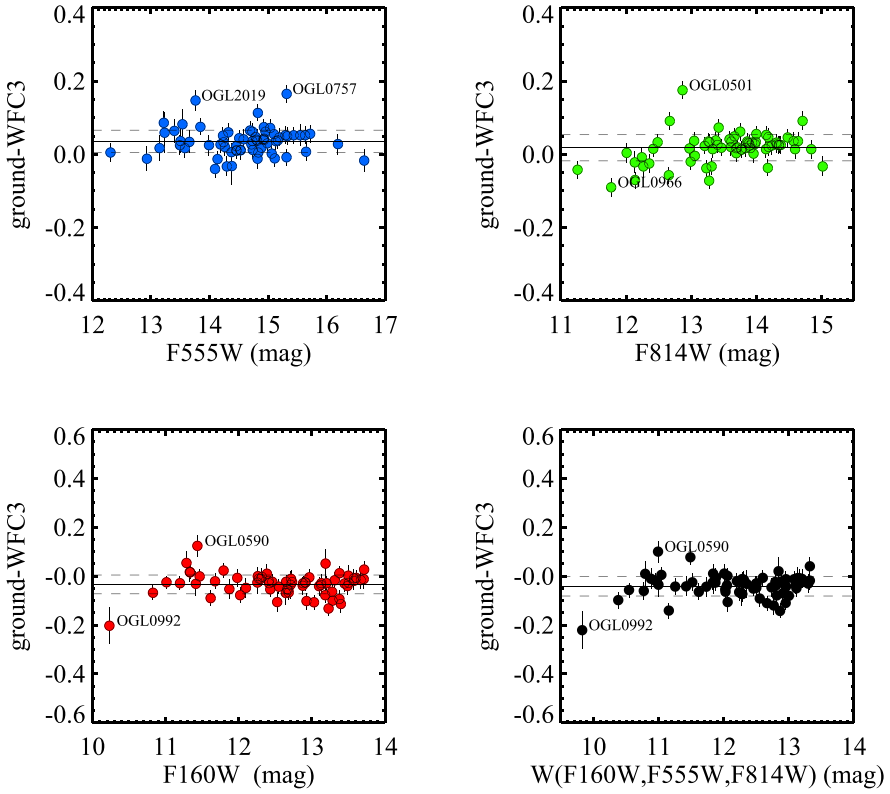

Figure 2. Comparison of Cepheid mean magnitudes in three *HST* WFC3 bands for observations obtained with *HST* and from the ground (transformed to the *HST* system).

plane geometry for the LMC with inclination $i = 25.^{\circ}0 \pm 4$ and position angle of the line of nodes $\Theta = 132^{\circ} \pm 10$ for a center of mass from van der Marel & Kallivayalil (2014) of $\alpha_0 = 80.^{\circ}05$, $\delta_0 = -69.^{\circ}30$. The mean correction for the DEBs to the center was 0.001 mag. For consistency with the geometry of the DEBs from Pietrzyński et al. (2019), we use the same model to correct the Cepheids to the center and mean DEB. Because more of our Cepheids are southwest of the line of nodes (which is tilted away from us), our mean Cepheid, according to the model, is more distant than the center by 0.011 mag (SD = 0.010 mag), with a full range of 0.004 mag closer to 0.038 mag more distant. The values of m_H^W in Table 2 include these individual corrections to account for the projected distance of the Cepheids from the line of nodes. To evaluate the systematic uncertainty in this correction, we consider other geometries. van der Marel & Kallivayalil (2014) used kinematic constraints to derive an inclination of $i = 26.^{\circ}2$ and position angle of the line of nodes $\Theta = 154.^{\circ}5$, which produced a mean correction for our Cepheids of 0.013 mag. An alternative model derived from the positions and fluxes of 2000 LMC Cepheids by Nikolaev et al. (2004), with $\alpha_0 = 79.^{\circ}4$, $\delta_0 = -69.^{\circ}03$, $i = 30.^{\circ}7$, and $\Theta = 151.^{\circ}0$, yields a mean correction of 0.016 mag. We will consider the standard deviation of these three models, 0.002 mag, to be a systematic uncertainty associated with the geometry of the LMC. As we will show, this term is subdominant to other error terms.

3. Period–Luminosity Relations

In Figure 3 we show the relations between Cepheid period and magnitudes in *F*555*W*, *F*814*W*, and *F*160*W* as well as two Wesenheit indices, $m_H^W = m_{F160W} - 0.386(m_{F555W} - m_{F814W})$ and $m_I^W = m_{F814W} - 1.3(m_{F555W} - m_{F814W})$. The slopes of these relations (Table 3) match well those derived from larger ground-based samples of LMC Cepheids from Soszynski et al. (2008) and M15. We determined the intercepts and scatter for m_H^W from a 2.7σ clipped mean (this threshold is derived from Chauvenet's criterion where we expect 0.5 outliers at $>2.7\sigma$ from a normal distribution with $N = 70$ Cepheids). The m_H^W relation gives the lowest scatter, SD = 0.075 mag, with only two marginal outliers, OGL0992 and OGL0847, at 2.8 and 3.1σ, respectively (including both of these outliers results in a slightly increased SD = 0.086). For the same set of Cepheids, their ground-based magnitudes transformed to m_H^W give a somewhat higher scatter of 0.084 (or 0.103 with no outliers removed); the increased scatter may be due, in part, to occasional light contamination from nearby stars in the lower quality images from the ground. To determine the intrinsic scatter in the *HST*-based relations we subtract the estimated measurement errors, finding a result of 0.069 mag (equivalent to 3.2% in distance) for a single Cepheid, which is at or near defining the lowest apparent dispersion of any known sample of Cepheids.

The scatter, after removing the same two outliers as above, is seen to decline with increasing wavelength, as may be expected because of the reduced impact of differential extinction and the narrower intrinsic width of the *P*–*L* relation. Two of the

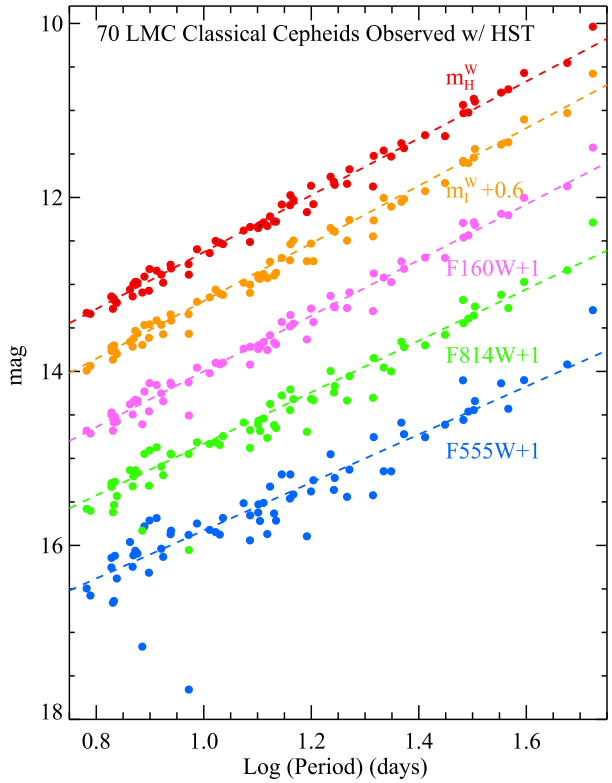

Figure 3. Period–mean magnitude relation for the 70 LMC Cepheids with slopes and statistics given in Table 3.

Table 3
Period–Mean magnitude Relations from *HST* LMC Cepheids

Band	Slope[a]	Intercept[b]	Scatter[b]
F555W	−2.76	17.638	0.312
F814W	−2.96	16.854	0.202
F160W	−3.20	16.209	0.104
m_I^W[c]	−3.31	15.935	0.085
m_H^W	−3.26	15.898[d]	0.075

Notes.
[a] From Soszynski et al. (2008), M15 and R16.
[b] Outliers are OGL0992 and OGL0847.
[c] $R = A_I/(A_V - A_I) = 1.3$ from Cardelli et al. (1989) $R_V = 3.1$ as Freedman et al. (2001).
[d] Includes CRNL.

Cepheids are particularly red, with $F555W - F814W$ of 1.3 and 1.6 mag for OGL1945 and OGL1940, respectively, or more than 3σ redder than the mean ($\langle F555W - F814W \rangle = 1.00$, SD = 0.09 without these two), but neither are outliers in the reddening-free m_H^W.

Although the Cepheid ground sample from M15 is an order of magnitude larger in size than the one observed with *HST*, the latter is more heavily weighted toward longer period Cepheids, which offers advantages when comparing to Cepheids in SN Ia hosts. The *HST* LMC sample has a mean period of 16 days ($\log P = 1.21$) and 45 Cepheids with $P > 10$ days, while the M15 ground sample has a mean period of 6.7 days ($\log P = 0.83$) and 109 Cepheids with $P > 10$ days. The mean Cepheid period in the SN Ia hosts is $\log P \sim 1.5$ (R16), so the difference in sample mean log P for the *HST* sample is less than half the ground sample. Thus, an uncertainty in the slope of the Cepheid P–L relation will propagate less than half the error in H_0 from the *HST* sample as from the ground sample.

Table 4
Systematic Error Budget for the LMC Cepheid Distance Ladder Calibration

Error	Value	Source
LMC P–L Mean	0.42%	measured here
DEB Mean	1.20%	Pietrzyński et al. (2019)
CRNL Across 4 dex	0.11%	Riess et al. (2019)
LMC Geometry	0.09%	std dev of 3 geometries (see text)
Photometry Methods	0.14%	measured here
Total	1.28%	

The formal error in the LMC Cepheid sample mean m_H^W is 0.0092 mag, equivalent to 0.42% in distance. The total formal uncertainty for the Cepheid LMC calibration is obtained by combining this uncertainty with the 0.0263 mag (or 1.20% in distance) error from the DEBs (Pietrzyński et al. 2019), the 0.0024 mag systematic uncertainty in the CRNL correction, the 0.003 mag difference between methods of measuring photometry, and the 0.002 mag uncertainty due to the LMC geometry. Together these yield a total uncertainty of 1.28% for the geometric calibration of the Cepheid distance ladder and H_0, which is the smallest error for any Cepheid calibration to date (see Table 4). Additional uncertainty when comparing these Cepheids to those with different metallicity or mean period will be considered in the next section.

Previous studies (Bhardwaj et al. 2016, and references therein) have suggested a change in slope of the P–L at $P = 10$ days at optical wavelengths, though its significance has been marginal and debated. As in R16, our primary fit for H_0 in the next section allows for a change in slope at $P = 10$ days; if the change in slope is real, not allowing for this degree of freedom in the solution could otherwise introduce a systematic error when comparing samples of Cepheids with differing mean periods. However, R16 found no evidence of a break in the m_H^W relation with slopes of -3.25 ± 0.02 and -3.26 ± 0.02 mag/dex below and above $P = 10$ days, respectively, averaged across all extragalactic Cepheids (including the 785 LMC Cepheids from M15). For only the 70 LMC Cepheids studied here, there is a slope difference of $\Delta = 0.20 \pm 0.30$ mag/dex across $P = 10$ days with the measured slope at $P > 10$ days ($N = 43$) of -3.38 ± 0.07 mag/dex, which is 2.1σ steeper than the R16 mean of extragalactic Cepheids. Because the sample is relatively small, the slope is sensitive to the low number of rare long-period Cepheids. Persson et al. (2004) measured a similar number ($N = 39$) of $P > 10$ day LMC Cepheids from the ground in the H-band and found a slope of -3.16 ± 0.10 mag/dex; they included two Cepheids at $P = 99$ and 134 days, neither of which was observed here and which pull the slope to lower values. The opposite has been seen for Cepheids in M31, with the longer period end being $\sim 2\sigma$ shallower than the shorter period end, though the combination produces no evidence of a break to 0.02 mag uncertainty (R16 and Kodric et al. 2015). As in R16, allowing for a break slightly reduces H_0 by 0.4% and is included, with other variants pertaining to the fitting of the P–L relation, in the systematic error.

4. The Hubble Constant

Following the distance ladder and additional constraints provided in R16, we can use this LMC Cepheid *P–L* relation to help calibrate the luminosity of SNe Ia and determine the value of H_0. Among the three geometric sources previously used by R16 for this purpose, masers in NGC 4258, MW parallaxes, and LMC DEBs, the latter yielded the lowest individual value of H_0, $72.04 \pm 2.67\,\mathrm{km\,s^{-1}\,Mpc^{-1}}$. This LMC-derived calibration employed 785 Cepheids observed from the ground from M15 and the eight DEBs from Pietrzyński et al. (2013). R16 assumed a systematic uncertainty between the ground and *HST*-based zero-point of $\sigma = 0.03$ mag, an estimate in good agreement with the empirical result of a 0.04 mag ground-to-space difference found in Section 2. This relative zero-point error limited the available precision well above the apparent error in the mean distance of the LMC Cepheid ground sample of $0.08\,\mathrm{mag}/\sqrt{785}$ or 0.003 mag, an order of magnitude lower than the zero-point uncertainty. This uncertainty was also significant compared to the previous LMC distance uncertainty from Pietrzyński et al. (2013) of 0.045 mag, resulting in a combined error of 0.054 mag from the prior LMC calibration route.

Here we use both the ground and *HST* sample of LMC Cepheids together, as each provides an important and complementary constraint. The 70 LMC Cepheids observed with *HST* alone constrain the error in the mean relative to Cepheids observed by *HST* in SN Ia hosts to a precision of just under 0.01 mag. After including the 0.0263 mag uncertainty of the DEB-based distance from Pietrzyński et al. (2019) and the uncertainty from the CRNL, the total error becomes 0.028 mag (1.28% in distance; see Table 4), about half the uncertainty of the LMC combination used in R16. The much larger ground-measured sample is still very valuable, considered simultaneously, to constrain the slope of the *P–L*. The slope was constrained in R16 from the ground-based sample to $\sigma \sim 0.01\,\mathrm{mag/dex}$ (or $\sigma \sim 0.02\,\mathrm{mag/dex}$ for two slopes if a break was allowed), which is independent of its $\sigma = 0.03$ mag zero-point uncertainty. Fitting the distance ladder with the system of equations given in R16 and retaining the systematic zero-point uncertainty for only the ground-based sample optimally leverages both samples. For each Cepheid with a ground and space-based measurement, we include a covariance term equal to the square of the intrinsic LMC dispersion measured here of 0.07 mag to account for this correlated error.

For the ground-based sample, we include the differences in projected distance to the line of nodes using the model of Pietrzyński et al. (2019) and their mean LMC distance of $\mu = 18.477 \pm 0.0263$ mag based on the DEBs, which have already been corrected to the line of nodes. For all LMC Cepheids, we assume a mean $[\mathrm{Fe/H}] = -0.30$ dex, which is chosen to be between the mean of -0.33 dex from 22 objects observed spectroscopically by Romaniello et al. (2008) and -0.27 dex, which is the mean of the photometric metallicity map of Choudhury et al. (2016) at the positions of the Cepheids from M15. This is slightly different than the value of -0.25 dex adopted by R16. Following Anderson & Riess (2018), we have also included a small correction of 0.0074 mag for the additional mean flux statistically and physically associated with Cepheids that is not resolved at the distances of the SN Ia hosts but that is resolved in the closer LMC, as discussed in Section 4. This is in addition to the use in R16 of artificial star measurements to account for mean additional light due to chance superposition on crowded backgrounds.

Table 5
Best Estimates of H_0 Including Systematics

Anchor(s)	Value ($\mathrm{km\,s^{-1}\,Mpc^{-1}}$)	Δ Planck[a]+ ΛCDM (σ)
LMC	74.22 ± 1.82	3.6
Two anchors		
LMC + NGC 4258	73.40 ± 1.55	3.7
LMC + MW	74.47 ± 1.45	4.6
NGC 4258 + MW	73.94 ± 1.58	3.9
Three anchors (preferred)		
NGC 4258 + MW + LMC	74.03 ± 1.42	4.4

Note.
[a] $H_0 = 67.4 \pm 0.5\,\mathrm{km\,s^{-1}\,Mpc^{-1}}$ (Planck Collaboration et al. 2018).

Using only the LMC distance from Pietrzyński et al. (2019) to geometrically calibrate the Cepheid luminosities, we find $74.22 \pm 1.82\,\mathrm{km\,s^{-1}\,Mpc^{-1}}$ including its systematic uncertainty calculated by the analysis variants method given in R16. The value is higher than the value of $72.04 \pm 2.67\,\mathrm{km\,s^{-1}\,Mpc^{-1}}$ from R16 by $2.2\,\mathrm{km\,s^{-1}\,Mpc^{-1}}$ (about 0.8σ or 2.9%) due primarily to the 1% decrease in the LMC distance between Pietrzyński et al. (2013, 2019) (which increases H_0 by 1%) and a ~2% increase from the use of the *HST* photometric system for the Cepheids. The overall uncertainty in H_0 using the geometric LMC calibrations has declined by 40%, 25% because of the improved LMC distance and 15% because of the use of a single photometric system, which nullifies the relative zero-point uncertainty. Because the LMC Cepheids have a lower metallicity than those in SN Ia hosts (or the MW or NGC 4258), there is an additional uncertainty of 0.9% when using the LMC as an anchor due to the uncertainty in the empirically constrained luminosity–metallicity relation. These improvements together make the LMC, with a 2.4% total uncertainty in H_0, comparable in precision (actually better) as an anchor of the distance ladder to the use of all MW Cepheid parallaxes, with the masers in NGC 4258 somewhat lower at 3.4% uncertainty; all are individually consistent within 1.3σ in terms of their independent geometric distance uncertainties.

In Table 5 we also list the result of combining the LMC with the MW Cepheid parallaxes (R18a), with the masers in NGC 4258, and every combination of using only a pair of anchors. These two-anchor (or one-anchor-out) combinations now have a smaller range of $1.07\,\mathrm{km\,s^{-1}\,Mpc^{-1}}$ (compared to $2.42\,\mathrm{km\,s^{-1}\,Mpc^{-1}}$ in R16) because of the increase in the result from the LMC. Indeed, leaving out any one of three anchors by choice, which is a reasonable test of robustness, changes H_0 by only $\sim 0.5\,\mathrm{km\,s^{-1}\,Mpc^{-1}}$ or <0.7%. For those inclined to disfavor any one anchor, these combinations offer a best result without the influence of the given anchor.

However, the best and preferred result comes from including all three anchors, giving $74.03 \pm 1.42\,\mathrm{km\,s^{-1}\,Mpc^{-1}}$, a total uncertainty of 1.91% including systematics. Compared to the predicted value of H_0 of $67.4 \pm 0.5\,\mathrm{km\,s^{-1}\,Mpc^{-1}}$ from the Planck Collaboration et al. (2018) CMB data in concert with the cosmological model, ΛCDM, this measurement differs by 4.4σ ($P = 99.999\%$), as shown in Figure 4.

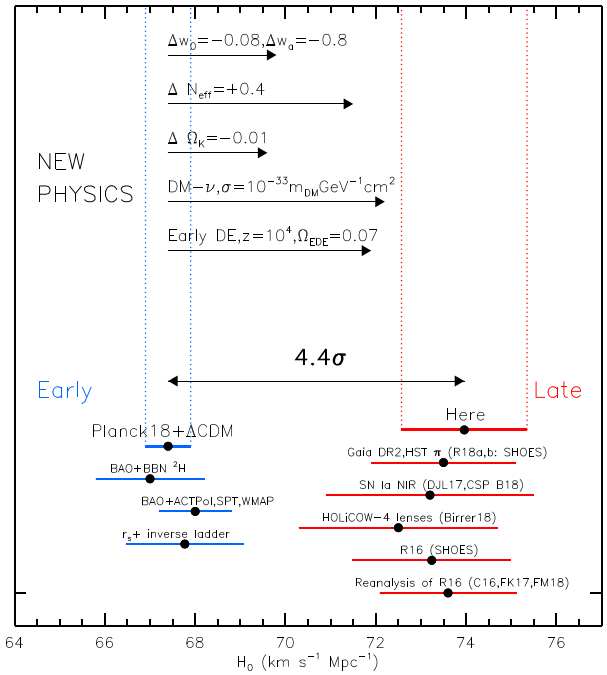

Figure 4. The 4.4σ difference between local measurements of H_0 and the value predicted from *Planck*+ΛCDM. We show local results presented by Riess et al. (2016), reanalysis by C16 (Cardona et al. 2017), FK17 (Follin & Knox 2018), or FM18 (Feeney et al. 2017), the HOLiCOW lensing results from Birrer18 (Birrer et al. 2018), a replacement of optical SN data with NIR in DJL17 (Dhawan et al. 2018) and B18 (Burns et al. 2018), and a revised geometric anchor from *HST* and *Gaia* DR2 parallaxes (R18a, b). Other early universe scales are shown in blue. Possible physics causes for a 2%–4% change in H_0 include time-dependent dark energy or nonzero curvature, while a larger 5%–8% difference may come from dark matter interaction, early dark energy or additional relativistic particles.

In Table 6 and Figure 5 we give a detailed breakdown of all sources of uncertainty in the determination of H_0 here and compared to R16. The primary changes between the present uncertainties in H_0 and those in R16 result from improvements in the anchor measurements from the LMC and MW. The contributed uncertainty from MW Cepheid parallaxes has decreased from 2.5% to 1.7% because of new parallax measurements from *HST* spatial scanning (R18b) and from *Gaia* Data Release 2 (R18a) and from the use of WFC3 to measure their photometry on the same photometric system as Cepheids in SN Ia hosts. These improvements in the MW anchor alone reduced the overall uncertainty in H_0 from 2.4% to 2.2% (R18a). An even greater improvement in the LMC anchor is now realized, decreasing its contributed uncertainty from 2.6% to 1.5%. While there is a small increase in uncertainty in the *P*–*L* intercept because of the smaller sample of LMC Cepheids here, this is more than offset by the smaller systematic uncertainty in their photometric zero-point. We also note that there is an increase in the overall uncertainty due to the relation between Cepheid metallicity and luminosity. The metallicity term we derived from our analysis of all Cepheid data (R16) is -0.17 ± 0.06 mag per dex, similar to Gieren et al. (2018), who find -0.22 mag per dex in the NIR for a lower range of metallicity. The product of the mean, subsolar metallicity for the LMC Cepheids and the uncertainty in this term is 0.9%. The other two anchors have Cepheids with near solar metallicities that are much closer to those in the SN hosts, so the overall uncertainty in H_0 due to metallicity is weighted down by these anchors to 0.5%.

5. Discussion

5.1. Systematics: Cepheid Associated Flux

The photometric measurements of Cepheids from R16 in SN Ia hosts and NGC 4258 account for the mean additional light due to chance superposition on crowded backgrounds through the use of artificial star measurements. However, the possibility of light from stars that are physically associated with the Cepheids and unresolved at their distances for SN Ia hosts (5–40 Mpc) but that is resolved in the LMC at 50 kpc (or the MW at 2–3 kpc), and thus excluded from measurement, would have a differential effect that could bias the determination of H_0. Anderson & Riess (2018) quantified this "associated-light bias" by studying its two plausible sources, wide binaries ($a_{\rm rel} > 400$ au) and open clusters (closer binaries are unresolved in all cases). They found that the mean effect of wide binaries was negligible (0.004% in H_0) because Cepheids dominate companions in luminosity. Closer binaries, while more common, are unresolved in either anchor galaxies or SN hosts, so even the tiny contamination of Cepheid flux from a companion, ∼0.02% in distance, cancels along the distance ladder because of its presence for all Cepheids (assuming binarity is common in all hosts). To quantify the impact of open clusters, they analyzed the regions around a large sample of Cepheids in M31, 450 Cepheids with UV *HST* imaging from the PHAT program (Dalcanton et al. 2012). They found that 2.4% of Cepheids are in such clusters and that the photometric bias averaging over Cepheids in or out of clusters is 0.0074 mag for m_H^W. This value might be considered an upper limit to the bias because there is also a "discovery bias" to exclude even the small fraction of Cepheids in bright clusters from a distant sample. The additional constant flux that is unresolved for distant Cepheids in clusters would decrease the amplitude of Cepheid light curves. Anderson & Riess (2018) found that a mean bias for a Cepheid in a cluster in M31 of 0.30 mag in m_H^W corresponds to a bias of 0.8 mag at visual wavelengths, near or brighter than the limit of 0.5 mag contamination that Ferrarese et al. (2000) determined would preclude discovery of a Cepheid because of the flattening of its light curve. In the other direction, one might posit a somewhat larger clustered fraction in SN Ia hosts than in M31 (M31 being somehow unusual), but this direction is limited by the greater ages of Cepheids (30–300 Myr) than clusters with only ∼10% of massive embedded clusters surviving for more than 10 Myr (Anderson & Riess 2018, and sources within). Indeed, M31 provides the best analog for the SN Ia hosts (high metallicity spiral) for which an up-close, external view of Cepheid environments is available. Such accounting for the MW may await improved parallaxes. In this regard, the LMC is unusual, with a greater frequency of Cepheids in clusters and a higher concentration of massive clusters (likely due to its high rate of recent star formation), with 7.2% of $P > 10$ day Cepheids in clusters (with fewer than four Cepheids per cluster). The LMC also harbors two Cepheid-rich clusters, each with 24 Cepheids, eight times the number of Cepheids as the richest MW cluster. Because of the great resolution of *HST* in the LMC, this excess of clusters around Cepheids in the LMC has no photometric impact on the measurement of H_0. Here we have included the expected impact of such flux based on the example of M31 and

Table 6
Recent H_0 Error Budgets (%)

Term	Description	Riess+ (2016)			Here		
		LMC	MW	4258	LMC	MW	4258
$\sigma_{\mu,\mathrm{anchor}}$	Anchor distance	2.1	2.1	2.6	1.2	1.5	2.6
$\sigma_{\mathrm{PL,anchor}}$	Mean of P–L in anchor	0.1	⋯	1.5	0.4	⋯	1.5
$R\sigma_{\lambda,1,2}$	Zero-points, anchor-to-hosts	1.4	1.4	0.0	0.1	0.7	0.0
σ_Z	Cepheid metallicity, anchor-hosts	0.8	0.2	0.2	0.9	0.2	0.2
	Subtotal per anchor	2.6	2.5	3.0	1.5	1.7	3.0
All Anchor subtotal			1.6			1.0	
$\sigma_{\mathrm{PL}}/\sqrt{n}$	Mean of P–L in SN Ia hosts		0.4			0.4	
$\sigma_{\mathrm{SN}}/\sqrt{n}$	Mean of SN Ia calibrators (# SN)		1.3 (19)			1.3 (19)	
σ_{m-z}	SN Ia m–z relation		0.4			0.4	
σ_{PL}	P–L slope, $\Delta\log P$, anchor-hosts		0.6			0.3	
Statistical error, σ_{H_0}			2.2			1.8	
Analysis systematics[a]			0.8			0.6	
Total uncertainty on σ_{H_0} [%]			2.4			1.9	

Note.
[a] Systematic errors calculated as standard deviation of 23 analysis variants presented in R16, given here as 1.48*median[abs(variants-mean(variants))].

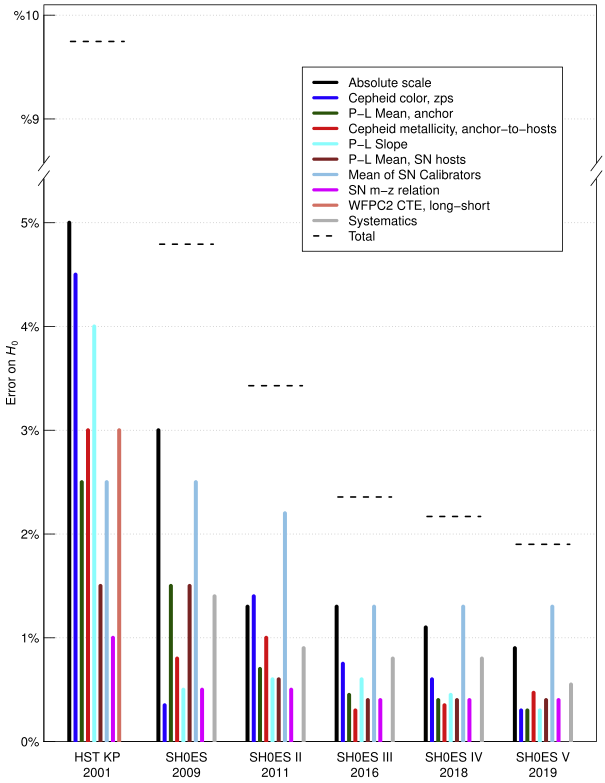

Figure 5. Evolution of error budgets for SH0ES distance ladder and a comparison to the *HST* Key Project Freedman et al. (2001). Each error source (length of bar) contributes in quadrature (its square) to the total error, thus larger errors will be more dominant than the visual (linear) comparison suggests.

conclude that it does not produce an impediment to measuring H_0 to 1%. Higher resolution imaging in the future from *James Webb Space Telescope* or large ground-based telescopes with adaptive optics may allow for measuring the fraction of Cepheids in clusters in more distant galaxies.

5.2. *Prospects for Reducing the* H_0 *Uncertainty: SN Statistics and Systematics*

As shown in Table 6 and Figure 5, with the new LMC anchor measurements in hand, the single largest source of uncertainty in H_0 now lies in determining the mean luminosity of the SN Ia calibrators. Future reductions in the uncertainty in H_0 will require increasing the number of these calibrations. The sample in R16 had 19 calibrators that were chosen according to SN Ia light-curve quality requirements and for their presence in nearby ($z \leqslant 0.01$), late-type, globally star-forming, nonedge on hosts that would thus be expected to yield a good sample of Cepheids. New observations with *HST* by the SH0ES program are underway, which will double this sample to 38 calibrators, making the sample complete to $z \sim 0.011$, and will reduce the uncertainty in this term by $\sqrt{2}$ and the likely overall error on H_0 to $\sim$1.5%.

With the prospect of reaching subpercentage uncertainty in the mean of SN Ia calibrators, even greater attention must be given to controlling potential systematic uncertainties in the measurement of SN Ia distances. One path to both better standardize SN Ia brightnesses and control systematics has been to search for additional observables that may correlate with distance residuals beyond light-curve shapes (Phillips 1993) and colors (Riess et al. 1996; Tripp 1998; Phillips et al. 1999). As the statistical leverage of larger and better calibrated SN samples has grown (Betoule et al. 2014; Scolnic et al. 2018), evidence has arisen of an environmental parameter that appears to correlate with SN distance residuals, albeit at a lower level than the preceding SN parameters. The most widely used form for this environmental parameter is to use the host galaxy mass as done by nearly all recent cosmology analyses including those from the SNLS (Sullivan et al. 2011), the Joint SNLS-SDSS Light Curve Analysis (JLA; Betoule et al. 2014), Pan-Starrs (Rest et al. 2014; Scolnic et al. 2014, 2018; Jones

et al. 2018b), SCP (Suzuki et al. 2012), Dark Energy Survey (DES Collaboration et al. 2018), SH0ES (R11, R16), and CSP (Burns et al. 2018). More recent studies have found a weaker (Scolnic et al. 2018) or absent (DES Collaboration et al. 2018) environmental dependance compared to past studies (Hicken et al. 2009; Kelly et al. 2010; Lampeitl et al. 2010; Sullivan et al. 2010), likely due to improved accounting for SN selection bias (Kessler & Scolnic 2017). Likewise, recent measurements of H_0 by R16 and Burns et al. (2018) have followed this approach and corrected for the empirical dependence of host mass in their samples.

We can evaluate the systematic error resulting from SN Hubble residual dependence on a different environmental parameter, such as star formation rate, colors, metallicity and population ages. An environmental parameter can impact the determination of the Hubble constant if two conditions are met: (1) the parameter has a significant relationship with the distance residuals for the same SN sample and method of distance determination used to measure the Hubble constant and (2) there is a mean difference in the parameter between the SNe in Cepheid hosts and those used to calibrate the Hubble expansion. Jones et al. (2018a) looked for additional environmental dependencies in the same SN sample and distance fitting method used by R16 to determine H_0 (the only such study of the R16 sample) including local and global color (in the UV to address star formation), local and global mass, and local specific star formation (suggested by Rigault et al. (2018) to relate to environmental age). They found that none of these is significant ($<2\sigma$) in the R16 distance residuals (which already include a correction for host mass and SN selection bias) with the possible exception of local mass ($\sim 3\sigma$). Significance aside, Jones et al. (2018a) combined the sample differences and size of the dependencies and for different environmental parameters they found an impact on H_0 of 0.3% to 0.5%. Roman et al. (2018) also found no significant relation between Hubble residuals and local SN UV color for 123 SNe Ia at $z < 0.1$ (1.7σ without a host mass correction). In a study of SDSS SNe Ia, Rose et al. (2019) performed a principal component analysis to create the optimal combination of multiple additional parameters that could correlate with distance residuals, finding an additional correlation between the inferred environmental age and Hubble residuals with 2.1σ significance, which would produce a $\sim$0.4% change to H_0 (after accounting for the present host mass correction, which is included in R16) if the same correlation exists in the nearby SNe used in R16. These residual environmental dependencies are much smaller than the present overall uncertainty, of low significance, and if true, would remain subdominant to the future statistical uncertainty in H_0 with a larger sample size of SN Ia calibrators.

The safest path to avoid possible (even unknown) environmental systematics would be to eliminate the potential cause for a mean difference in environments between the SNe in Cepheid hosts and those used to calibrate the Hubble expansion by employing the same criteria to select SNe in the two relevant samples. A simple approach would be to limit SNe in the Hubble Flow sample to those in globally late-type, star-forming hosts. These are the same criteria used to select likely Cepheid hosts, and because the nature of the local SN environment is not relevant and, thus, is not a factor in this selection, the statistics of local environments would be similar in both samples. R16 employed both a late-type only and globally star-forming only selection as a variant for the determination of H_0 and demonstrated a change of $H_0 < 0.3\%$.

The advantage of this approach is illustrated in the study of Hα local to the SN site. In studies of the unpublished SN Factory sample, Rigault et al. (2013, 2018) suggested that the presence of local Hα, a consequence of a very young population, may have an important dependence on SN distance with strong Hα (for a specific local mass) producing fainter SNe (a similar effect as having a low mass host). Because the Hubble flow sample may include SNe with early-type hosts with lower local Hα, a higher mean local Hα may be expected in the purely late-type (and globally star-forming) hosts of the Cepheid calibrator sample. Thus, if a local Hα relation existed in the SN sample used to determine H_0, it could erroneously raise its measured value. However, including only late-type hosted SNe in the Hubble flow sample would remove the underlying cause of such a bias. Anderson et al. (2015) provide measurements of the relative strength of Hα at the sites of 98 SNe Ia in exclusively late-type, star-forming hosts, including 20 of the 38 selected for Cepheid measurements, which can be used to test this approach. Of the selected Cepheid hosts, 14 of 20 (70%) (or 8 of 11 from R16) have no detected Hα (at the 0% level relative to the host), while in the non-Cepheid selected sample, 43 of 78 (55%) show no Hα. The mean of the Cepheid sample is, thus, consistent with (albeit lower in) Hα, demonstrating that limiting the samples to the same host type removes the source of a sample mean difference of Hα to the level expected from statistical fluctuations (or another factor unrelated to selection). This negates the potential for biasing the value of H_0, whether or not a dependence exists in the R16 Hubble flow sample (which has not been shown). In this case, an even balance of SNe with high, local Hα among late-type, star-forming hosts is expected because the presence of SN local Hα never enters their selection. Limiting the Hubble flow sample to the same criteria as Cepheid hosts reduces the sample by less than half and thus has little impact on the precision of H_0.

5.3. Present Status

The recent landscape of model-independent, direct measurements of H_0 from the late universe and predictions from the early universe is shown in Figure 4. While it is difficult and perhaps debatable to identify the precise threshold at which a tension passes the point of being attributable to a fluke, the one presently involving H_0 appears to have passed that point.[7]

The higher, local value of H_0 from the distance ladder has been determined through five independent geometric absolute calibrations of the Cepheid P–L relation, including new MW parallaxes from *HST* spatial scans (R18b) and from *Gaia* DR2 (R18a). As shown in Table 5, any one of the three types of anchors can be removed with a change in H_0 of $<0.7\%$, much smaller than the present 9% discrepancy. The relative distances from Cepheids match those from the Tip of the Red Giant Branch (Jang & Lee 2017; Jang et al. 2018; Hatt et al. 2018b, 2018a) and Miras (Huang et al. 2018; Yuan et al. 2017)

[7] In the search for a new particle where an unexpected "bump" in events may occur at any point along a continuum of energies, the "Look Elsewhere" effect of having too many chances (bins) for a random fluctuation to appear is typically overcome with a high threshold for significance, usually 5σ. Here where we have only one cosmological parameter (or at most a few) to compare between the early and late universe, and only one universe to observe, fewer throws of the dice are possible, so we consider the present discrepancy quite significant.

to a mean precision of 2%–3%. Strong-lensing results from the HOLiCOW team have corroborated the local value of H_0 independent of the distance ladder (Birrer et al. 2018). At the other end of cosmic time, the low expected value of H_0 predicted from the early universe has been confirmed by different sources of CMB and BAO data and by an independent calibration of BAO from measurements of Ω_B and knowledge of the CMB temperature (Addison et al. 2018). It is important to note that "inverse distance ladders" and calibrations of BAO or SNe originating from the sound horizon ($z \sim 1000$) or from CMB measurements all fall into this "early universe" category of H_0 inference. With multiple, independent corroborations now demonstrated at both ends of cosmic history, we may need to seek resolution in a refinement of the model that joins them, (Vanilla) ΛCDM.

A new feature in the dark sector of the universe appears increasingly necessary to explain the present difference in views of expansion see from the beginning or from the present. The general considerations by Aylor et al. (2018) argue for an injection of energy or expansion preceding recombination, which would shorten the time for the Universe to become transparent and reduce the sound horizon inferred from the CMB and used to calibrate BAO with a specific scenario offered by Poulin et al. (2018). The dark radiation sector (i.e., neutrinos) also provides a possible source for alleviation of the H_0 difference through interactions of additional components (Kreisch et al. 2019).

Continued pursuit in precision in the determination of H_0 is also needed to transition from the discovery of a difference to a diagnosis of its source. Additional observations of giants and pulsating stars in more hosts of SNe Ia are underway and should further refine H_0. Less predictable but highly sought are contributions from gravitational wave sources as standard sirens (Schutz 1986; Abbott et al. 2017; Chen et al. 2018). Improvements in parallaxes from future *Gaia* data releases are also expected to continue to increase the precision of the distance ladder in the near term.

We are grateful to Roeland van der Marel for assistance with the geometry of the LMC.

Support for this work was provided by the National Aeronautics and Space Administration (NASA) through programs Nos. GO-14648, 15146 from the Space Telescope Science Institute (STScI), which is operated by AURA, Inc., under NASA contract No. NAS 5-26555. A.G.R., S.C., and L. M.M. gratefully acknowledge support by the Munich Institute for Astro- and Particle Physics (MIAPP) of the DFG cluster of excellence "Origin and Structure of the Universe."

This research is based primarily on observations with the NASA/ESA *Hubble Space Telescope*, obtained at STScI, which is operated by AURA, Inc., under NASA contract No. NAS 5-26555.

The *HST* data used in this paper are available at 10.17909/t9-my41-h234 as part of the MAST archive which can be accessed at http://archive.stsci.edu/hst/.

ORCID iDs

Wenlong Yuan https://orcid.org/0000-0001-9420-6525
Lucas M. Macri https://orcid.org/0000-0002-1775-4859

References

Abbott, B. P., Abbott, R., Abbott, T. D., et al. 2017, Natur, 551, 85
Addison, G. E., Watts, D. J., Bennett, C. L., et al. 2018, ApJ, 853, 119
Anderson, J. P., James, P. A., Förster, F., et al. 2015, MNRAS, 448, 732
Anderson, R. I., & Riess, A. G. 2018, ApJ, 861, 36
Aylor, K., Joy, M., Knox, L., et al. 2018, ApJ, 874, 4
Barenboim, G., Denton, P. B., & Oldengott, I. M. 2019, arXiv:1903.02036
Benedict, G. F., McArthur, B. E., Feast, M. W., et al. 2007, AJ, 133, 1810
Betoule, M., Kessler, R., Guy, J., et al. 2014, A&A, 568, A22
Bhardwaj, A., Kanbur, S. M., Macri, L. M., et al. 2016, MNRAS, 457, 1644
Birrer, S., Treu, T., Rusu, C. E., et al. 2018, arXiv:1809.01274
Bohlin, R., & Deustua, S. 2019, , arXiv:1903.11985
Burns, C. R., Parent, E., Phillips, M. M., et al. 2018, ApJ, 869, 56
Calamida, A., Matheson, T., Saha, A., et al. 2018, ApJ, 872, 199
Cardelli, J. A., Clayton, G. C., & Mathis, J. S. 1989, ApJ, 345, 245
Cardona, W., Kunz, M., & Pettorino, V. 2017, JCAP, 3, 056
Chen, H.-Y., Fishbach, M., & Holz, D. E. 2018, Natur, 562, 545
Choudhury, S., Subramaniam, A., & Cole, A. A. 2016, MNRAS, 455, 1855
Dalcanton, J. J., Williams, B. F., Lang, D., et al. 2012, ApJS, 200, 18
D'Eramo, F., Ferreira, R. Z., Notari, A., & Bernal, J. L. 2018, JCAP, 11, 014
DES Collaboration, Abbott, T. M. C., Allam, S., et al. 2019, ApJ, 872, 30
Dhawan, S., Jha, S. W., & Leibundgut, B. 2018, A&A, 609, 72
Di Valentino, E., Linder, E. V., & Melchiorri, A. 2018, PhRvD, 97, 043528
Feeney, S. M., Mortlock, D. J., & Dalmasso, N. 2018, MNRAS, 476, 3861
Ferrarese, L., Silbermann, N. A., Mould, J. R., et al. 2000, PASP, 112, 177
Fitzpatrick, E. L. 1999, PASP, 111, 63
Follin, B., & Knox, L. 2018, MNRAS, 477, 4534
Freedman, W. L., Madore, B. F., Gibson, B. K., et al. 2001, ApJ, 553, 47
Gieren, W., Storm, J., Konorski, P., et al. 2018, A&A, 620, A99
Hatt, D., Freedman, W. L., Madore, B. F., et al. 2018a, ApJ, 861, 104
Hatt, D., Freedman, W. L., Madore, B. F., et al. 2018b, ApJ, 866, 145
Hertzsprung, E. 1913, AN, 196, 201
Hicken, M., Wood-Vasey, W. M., Blondin, S., et al. 2009, ApJ, 700, 1097
Hoffmann, S. L., Macri, L. M., Riess, A. G., et al. 2016, ApJ, 830, 10
Huang, C. D., Riess, A. G., Hoffmann, S. L., et al. 2018, ApJ, 857, 67
Humphreys, E. M. L., Reid, M. J., Moran, J. M., Greenhill, L. J., & Argon, A. L. 2013, ApJ, 775, 13
Jang, I. S., Hatt, D., Beaton, R. L., et al. 2018, ApJ, 852, 60
Jang, I. S., & Lee, M. G. 2017, ApJ, 836, 74
Jones, D. O., Riess, A. G., Scolnic, D. M., et al. 2018a, ApJ, 867, 108
Jones, D. O., Scolnic, D. M., Riess, A. G., et al. 2018b, ApJ, 857, 51
Kalirai, J. S., MacKenty, J., & Bohlin, R. 2009, Instrument Science Report WFC3 2009-30
Kelly, P. L., Hicken, M., Burke, D. L., Mandel, K. S., & Kirshner, R. P. 2010, ApJ, 715, 743
Kessler, R., & Scolnic, D. 2017, ApJ, 836, 56
Khosravi, N., Baghram, S., Afshordi, N., & Altamirano, N. 2017, arXiv:1710.09366
Kochanek, C. S., Shappee, B. J., Stanek, K. Z., et al. 2017, PASP, 129, 104502
Kodric, M., Riffeser, A., Seitz, S., et al. 2015, ApJ, 799, 144
Kreisch, C. D., Cyr-Racine, F.-Y., & Doré, O. 2019, arXiv:1902.00534
Lampeitl, H., Smith, M., Nichol, R. C., et al. 2010, ApJ, 722, 566
Leavitt, H. S., & Pickering, E. C. 1912, HarCi, 173, 1
Macaulay, E., Nichol, R. C., Bacon, D., et al. 2019, MNRAS, 486, 2184
Macri, L. M., Ngeow, C.-C., Kanbur, S. M., Mahzooni, S., & Smitka, M. T. 2015, AJ, 149, 117
Madore, B. F. 1982, ApJ, 253, 575
Momcheva, I. G., van Dokkum, P. G., van der Wel, A., et al. 2017, PASP, 129, 015004
Mörtsell, E., & Dhawan, S. 2018, JCAP, 9, 025
Narayan, G., Matheson, T., Saha, A., et al. 2019, ApJS, 241, 20
Nikolaev, S., Drake, A. J., Keller, S. C., et al. 2004, ApJ, 601, 260
Pandey, K. L., Karwal, T., & Das, S. 2019, arXiv:1902.10636
Persson, S. E., Madore, B. F., Krzemiński, W., et al. 2004, AJ, 128, 2239
Phillips, M. M. 1993, ApJL, 413, L105
Phillips, M. M., Lira, P., Suntzeff, N. B., et al. 1999, AJ, 118, 1766
Pietrzyński, G., Graczyk, D., Gallenne, A., et al. 2019, Natur, 567, 200
Pietrzyński, G., Graczyk, D., Gieren, W., et al. 2013, Natur, 495, 76
Planck Collaboration, Aghanim, N., Akrami, Y., et al. 2018, arXiv:1807.06209
Pojmanski, G. 1997, AcA, 47, 467
Poulin, V., Smith, T. L., Karwal, T., & Kamionkowski, M. 2018, arXiv:1811.04083
Renk, J., Zumalacárregui, M., Montanari, F., & Barreira, A. 2017, JCAP, 10, 020
Rest, A., Scolnic, D., Foley, R. J., et al. 2014, ApJ, 795, 44

Riess, A. G. 2010, First On-orbit Measurements of the WFC3-IR Count-rate Non-Linearity ISR 2010-07
Riess, A. G. 2011, An Independent Determination of WFC3-IR Zeropoints and Count Rate Non-Linearity from 2MASS Asterisms ISR 2011-15
Riess, A. G., Casertano, S., Yuan, W., et al. 2018a, ApJ, 861, 126
Riess, A. G., Casertano, S., Yuan, W., et al. 2018b, ApJ, 855, 136
Riess, A. G., Macri, L., Casertano, S., et al. 2011, ApJ, 730, 119
Riess, A. G., Macri, L. M., Hoffmann, S. L., et al. 2016, ApJ, 826, 56
Riess, A. G., Narayan, G., & Calamida, A. 2019, Calibration of the WFC3-IR Count-rate Nonlinearity, Sub-percent Accuracy for a Factor of a Million in Flux ISR 2019-01
Riess, A. G., Press, W. H., & Kirshner, R. P. 1996, ApJ, 473, 88
Rigault, M., Brinnel, V., Aldering, G., et al. 2018, arXiv:1806.03849
Rigault, M., Copin, Y., Aldering, G., et al. 2013, A&A, 560, A66
Roman, M., Hardin, D., Betoule, M., et al. 2018, A&A, 615, A68
Romaniello, M., Primas, F., Mottini, M., et al. 2008, A&A, 488, 731
Rose, B. M., Garnavich, P. M., & Berg, M. A. 2019, ApJ, 874, 32
Sahu, K., Baggett, S., & MacKenty, J. 2014, Use of the Shutter Blade Side for UVIS Short Exposures ISR 2014-09
Sandage, A., Tammann, G. A., Saha, A., et al. 2006, ApJ, 653, 843
Schutz, B. F. 1986, Natur, 323, 310
Scolnic, D., Rest, A., Riess, A., et al. 2014, ApJ, 795, 45
Scolnic, D. M., Jones, D. O., Rest, A., et al. 2018, ApJ, 859, 101
Shappee, B. J., Prieto, J. L., Grupe, D., et al. 2014, ApJ, 788, 48
Skrutskie, M. F., Cutri, R. M., Stiening, R., et al. 2006, AJ, 131, 1163
Soszynski, I., Poleski, R., Udalski, A., et al. 2008, AcA, 58, 163
Sullivan, M., Conley, A., Howell, D. A., et al. 2010, MNRAS, 406, 782
Sullivan, M., Guy, J., Conley, A., et al. 2011, ApJ, 737, 102
Suzuki, N., Rubin, D., Lidman, C., et al. 2012, ApJ, 746, 85
Szymanski, M. K. 2005, AcA, 55, 43
Tripp, R. 1998, A&A, 331, 815
Udalski, A., Szymanski, M. K., Soszynski, I., & Poleski, R. 2008, AcA, 58, 69
Udalski, A., Szymański, M. K., & Szymański, G. 2015, AcA, 65, 1
van der Marel, R. P., & Kallivayalil, N. 2014, ApJ, 781, 121
Vattis, K., Koushiappas, S. M., & Loeb, A. 2019, arXiv:1903.06220
Yuan, W., Macri, L. M., He, S., et al. 2017, AJ, 154, 149